Dalton Transactions

ROYAL SOCIETY OF CHEMISTRY

PAPER

View Article Online
View Journal | View Issue

Cite this: *Dalton Trans.*, 2026, **55**, 5679

Effect of alkyl substituent on the amide of bis-lactam-1,10-phenanthroline ligands for lanthanide extraction

Fengxin Gao,[a] Dong Fang *[b] and Chengliang Xiao *[a,b]

2,9-Diamide-1,10-phenanthroline (DAPhen) and bis-lactam-1,10-phenanthroline (BLPhen) ligands have been demonstrated to extract light lanthanides through size-specific coordination cavities selectively. Given that the alkyl chain has a substantial impact on the extraction performance of DAPhen, elucidating the role of the substituent chain for BLPhen is of great importance. In this study, four BLPhen ligands with varying alkyl substituents were synthesized to investigate the impact of alkyl chain length and branching on the extraction and coordination behavior toward trivalent lanthanides. Extraction studies demonstrate that the extraction trend for lanthanides was primarily governed by the size of the coordination cavity of BLPhen, and remained unchanged upon the introduction of variations in alkyl chain length or branching. However, ligands with shorter straight-chain alkyl groups (**L1**) exhibited optimal extraction efficiency and selectivity for light lanthanides, while increasing the alkyl chain length or incorporating branching led to a decline in performance. Slope analyses indicate variable metal-to-ligand stoichiometries for light, middle, and heavy lanthanide elements. UV–vis titration and ESI-MS analysis in homogeneous solution confirmed uniform 1 : 1 complexation for all metal–ligand systems. X-ray diffraction single-crystal structure provided clear coordination information, showing that coordination by the rigid ligand occurred without the need for conformational rotation, thereby minimizing energetic costs and enhancing complex stability. Overall, this study highlights the role of alkyl substituent geometry in modulating the coordination strength and selectivity of BLPhen ligands, providing a structural foundation for the rational design of highly efficient and preorganized extractants for rare earth separation.

Received 17th December 2025,
Accepted 16th March 2026

DOI: 10.1039/d5dt03012a

rsc.li/dalton

Introduction

Rare earth elements (REEs), comprising scandium (Sc), yttrium (Y), and the lanthanides (Lns), play a pivotal role in electronics, magnetic materials, metallurgy, medical applications, and catalysis owing to their unique electronic configurations and exceptional physicochemical properties.[1,2] With the rapid advancement of high-tech industries, the global demand for rare earth elements continues to increase, making them indispensable in numerous cutting-edge applications.[3,4] In addition to their significant market value, REEs have also emerged as critical resources in the global transition toward a greener and more sustainable economy.[5] However, REEs are typically found in nature as coexisting mixtures, and the lanthanide elements exhibit highly similar chemical characteristics, with most existing in the trivalent oxidation state, which renders their separation exceptionally challenging.[6,7] Therefore, it is urgently necessary to develop efficient, cost-effective, and environmentally sustainable technologies for separating trivalent lanthanides (Lns(III)),[8,9] which are critical for promoting the sustainable growth of green energy technologies.[10–12]

Currently, solvent extraction is widely used in industry as the primary method for separating various target metal ions.[13–15] This technique offers significant advantages, such as high processing capacity and relatively low energy consumption, making it the predominant approach for industrial lanthanide purification.[16] Although Lns(III) exhibit only minor variations in their chemical properties, these subtle variations can be effectively amplified through the rational design of ligands in combination with multistage or cascade extraction processes, enabling the stepwise separation of lanthanides within the series.[17–20]

Due to the gradual decrease in ionic radii across the lanthanide series and the corresponding increase in effective nuclear charge from La(III) to Lu(III), the well-known lanthanide contraction effect arises. As a result, most ligands tend to form

[a]*College of Chemical and Biological Engineering, Zhejiang University, Hangzhou 310058, China. E-mail: xiaoc@zju.edu.cn*
[b]*Institute of Zhejiang University-Quzhou, Quzhou, 324000, China. E-mail: fangdong1992@zju.edu.cn*

stronger coordination bonds with heavier lanthanides possessing higher effective nuclear charges, such as diglycolamide (DGA)[21] and tributyl phosphate (TBP).[22] In recent years, N,O-heterocyclic ligands based on the 1,10-phenanthroline scaffold have demonstrated great potential in the separation of f-block elements, which exhibit numerous distinctive and significant properties. Their affinities for lanthanides exhibited different trends across the series, including normal extraction, inverse extraction, and peak-shaped extraction centered in the middle of the series. For example, the saponified phenanthroline carboxamide ligand, 9-(*N*,*N*-dioctylcarbamoyl)-1,10-phenanthroline-2-sodium carboxylate (NaDOAPA, Fig. 1a), exhibited pronounced selectivity toward heavy lanthanides. At pH = 4, the $SF_{Lu(III)/La(III)}$ reached 787, enabling efficient discrimination of heavy lanthanides from their light and medium counterparts.[23] On the other hand, 2,9-bis(diphenylphosphine oxide)-1,10-phenanthroline (Ph_2-BPPhen, Fig. 1b) exhibited a non-monotonic trend in its extraction efficiency for Lns(III), with $D_{Eu(III)}$ exceeding both $D_{La(III)}$ and $D_{Lu(III)}$. The $\log\beta$ values obtained from UV–vis titration corroborated this observation, which has been attributed to the optimal size match between the ligand coordination cavity and Eu(III).[24] Moreover, for the phenanthroline diamide ligands (DAPhen, Fig. 1c), the extraction efficiency declined markedly as the lanthanide atomic number increased, with a preferential affinity toward light lanthanides (La(III), Ce(III), and Pr(III)), a behavior arising from their size selectivity.[25] Furthermore, changing the alkyl substituent can significantly influence the extraction behavior of the DAPhen ligands.[26–28] It has been demonstrated that the reduction of the alkyl substituent length from dodecyl to butyl led to over a fivefold enhancement in the ligand's extraction efficiency for f-block elements.[29,30] Leveraging the inherent advantages of preorganized ligands, bis-lactam-1,10-phenanthroline (BLPhen, Fig. 1d), derived from DAPhen, has demonstrated superior extraction performance toward f-block elements, while maintaining pronounced size selectivity for light lanthanides. Notably, BLPhen exhibited a sharp transition in extraction distribution ratios across the lanthanides, resulting in remarkable selectivity between light and heavy lanthanides, with $SF_{La(III)/Lu(III)}$ values exceeding 17 000.[31–33] However, these ligands decomposed rapidly under high acidity, limiting their potential applications. Thereafter, the more stabilized BLPhen was designed and synthesized, which overcame the stability issues of previous versions[34] and achieved $SF_{La(III)/Lu(III)}$ values consistently above 100.[35]

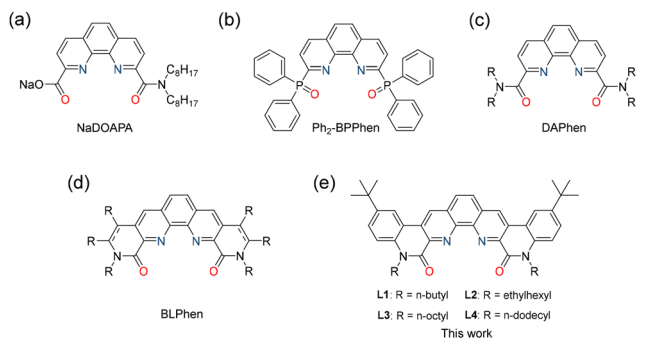

Fig. 1 Ligand structures of (a) NaDOAPA, (b) Ph_2-BPPhen, (c) DAPhen, (d) BLPhen, and (e) this work.

Although numerous studies have shown that the alkyl chain length on the amide group and the substituents on the aromatic ring significantly affect the extraction capacity of ligands,[36–38] it remains unclear the effect of alkyl substituent properties on the extraction performance of BLPhen. Herein, four BLPhen ligands (**L1–L4**, Fig. 1e) bearing amide functionalities with alkyl substituents of varying chain lengths were synthesized to evaluate the impact of alkyl structural variations on lanthanide extraction behavior. Ligands **L1**, **L3**, and **L4** featured linear alkyl chains, while **L2** incorporated a branched 2-ethylhexyl group. The extraction performance of these ligands toward lanthanides was systematically evaluated under different nitric acid and ligand concentrations. Additionally, UV–vis spectroscopy titration was employed to determine the stability constants ($\log\beta$) of the corresponding metal–ligand complexes in homogeneous solution. Detailed insights into the complexes were obtained from ESI-MS and single-crystal X-ray diffraction analyses. This work aims to elucidate the structure–property relationships governing ligand–lanthanide interactions, with particular focus on the role of amide alkyl substituents, thereby providing insights for the rational design of efficient and selective ligands for f-elements separation.

Results and discussion

Solvent extraction

Influence of HNO_3 concentration. To investigate the extraction behavior of the four ligands toward trivalent lanthanides, solvent extraction experiments were conducted over a range of HNO_3 concentrations (0.001–4.0 M), as presented in Fig. 2. All ligands exhibited similar trends, with extraction efficiency gradually decreasing from La(III) to Lu(III), indicating an inverse correlation between extractability and atomic number. Higher extraction efficiencies were observed for light lanthanides (La(III)–Nd(III)), whereas those of the heavy lanthanides (Ho(III)–Lu(III)) decreased markedly, typically below 10%. Moreover, the extraction performance of these ligands was also influenced by the HNO_3 concentration. For light lanthanides, maximum extraction occurred at 1.0–2.0 M HNO_3, while middle lanthanides showed peak extraction at 4.0 M. In contrast, no consistent trend was observed for heavy lanthanides due to the low extraction efficiency, resulting in significant experimental errors. These observations were consistent with the findings of Popova *et al.* on stabilized BLPhen,[35] further confirming that changes in the alkyl chain length of the amide substituent have little effect on the extraction sequence of Lns (III). Instead, the extraction behavior across the lanthanide series appeared to be primarily governed by the size of the coordination cavity. A notable exception was observed for Ce (III), which exhibited a lower extraction efficiency than Pr(III), despite having a lower atomic number. This deviation is likely

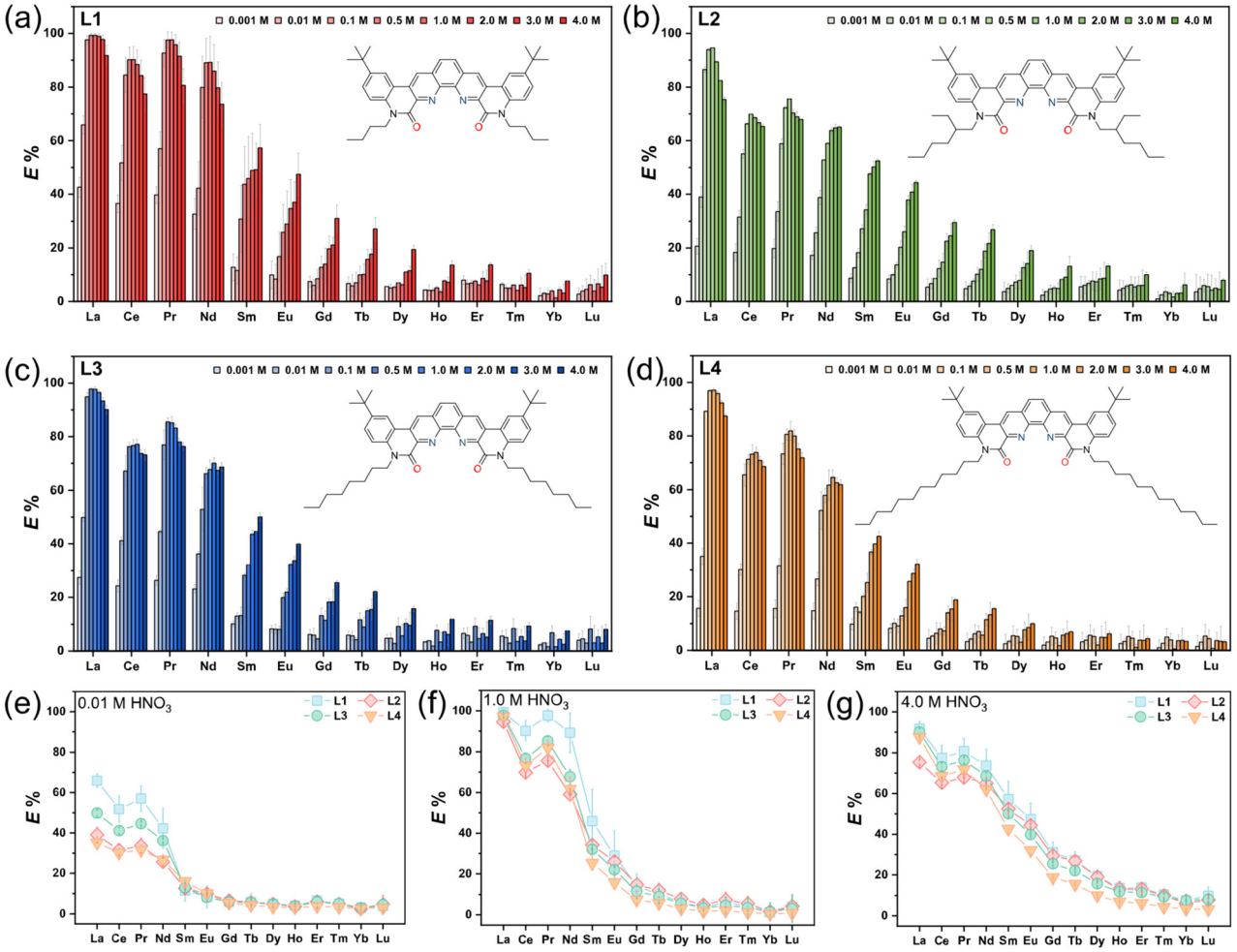

Fig. 2 Extraction of lanthanide elements by ligands (a) **L1**, (b) **L2**, (c) **L3**, and (d) **L4** under varying nitric acid concentrations. Extraction efficiencies of the ligands in (e) 0.01, (f) 1.0, and (g) 4.0 M HNO_3. [L] = 1.0 mM.

due to the partial oxidation of Ce(III) to Ce(IV) under ambient conditions, for which the ligands exhibit a weak binding affinity, thereby diminishing the overall extraction efficiency.[39] Among the four ligands, **L3** and **L4** exhibited a more distinct four-region extraction profile compared to **L1** and **L2**. Specifically, for the light lanthanides (La(III)–Nd(III)), extraction efficiency initially increased with acidity before declining; for the middle lanthanides (Sm(III)–Eu(III)), it rised continuously; for the middle lanthanides (Gd(III)–Ho(III)), it exhibited a rise–fall–rise trend; whereas for the heavy lanthanides (Er(III)–Lu (III)), extraction efficiency remained consistently low. On the other hand, the extraction behavior and separation performance of ligands **L1–L4** were evaluated at low, medium, and high HNO_3 concentrations (0.01 M, 1.0 M, and 4.0 M, respectively) as shown in Fig. 3e–g. At all three acid concentrations, the differences in extraction ability were primarily observed for the light lanthanides, following the order **L1** > **L3** > **L2** > **L4**. This suggests that the introduction of longer straight-chain alkyl groups may enhance the differentiation in lanthanide extraction behavior, and the incorporation of longer and

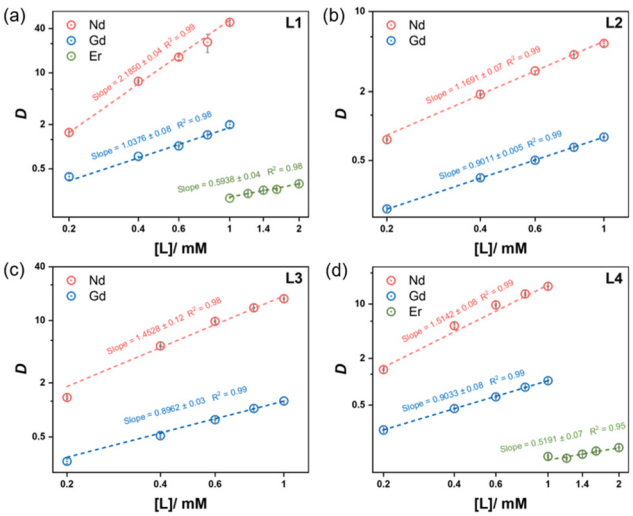

Fig. 3 Extraction slope experiment of (a) **L1**, (b) **L2**, (c) **L3**, and (d) **L4** for representative lanthanide elements. [HNO_3] = 1.0 M.

branched chains led to a decrease in extraction efficiency, likely due to the steric effects of the substituent.[40,41]

Nd(III), exhibiting the lowest extraction efficiency among the light lanthanides, and Ho(III), exhibiting the highest among the heavy lanthanides, were chosen as representatives of the light and heavy lanthanides, respectively. This selection was used to evaluate the ligands' separation performance for light *versus* heavy lanthanides and to assess the feasibility of group-wise lanthanide separation. The corresponding separation factors (SF) for Nd(III) over Ho(III) are shown in Fig. S11. Notably, under 1.0 M HNO_3, all ligands exhibited the strongest separation capability, with **L1** achieving the highest $SF_{Nd(III)/Ho(III)}$ (>500), followed by **L3** and **L4**, while **L2** displayed the lowest selectivity (>30). However, at 0.01 M and 4.0 M HNO_3, the $SF_{Nd(III)/Ho(III)}$ for all ligands were significantly reduced. These results suggest that moderate acidity (1.0 M HNO_3) provided the optimal conditions for balancing extraction efficiency and separation selectivity.

Overall, BLPhen enabled efficient separation between light and heavy lanthanides.

Influence of ligand concentrations. To further elucidate the extraction behavior of the ligands toward light, middle, and heavy lanthanides, slope analyses were conducted using Nd(III), Gd(III), and Er(III) as representative ions under varying ligand concentrations. The solubility of **L2** and **L3** in 1,2-DCE was limited to less than 1.5 mM. At low ligand concentrations, $D_{Er(III)}$ was too low, causing substantial experimental errors and hindering data fitting. Therefore, slope experiments for Er(III) could not be performed with these two ligands. As shown in Fig. 3, the slope values of Nd(III) ranged from 1 to 2.2 for all ligands, with **L1** exhibiting a slope of approximately 2, indicating the formation of a 2 : 1 ligand-to-metal complex. **L2–L4** yielded slope values between 1 and 2, suggesting a mixture of 1 : 1 and 2 : 1 complexes. Specifically, **L2** exhibited a slope closer to 1, suggesting that the 1:1 species was the predominant one, whereas **L3** and **L4** had intermediate slopes (~1.5), indicating the significant presence of both species. For ligands with linear alkyl substituents, increasing the chain length from butyl (**L1**) to octyl (**L3**) reduced the proportion of 2 : 1 complexes, likely due to increased steric hindrance, while further elongation to dodecyl (**L4**) had a minimal additional steric hindrance effect. In contrast, the branched substituent in **L2** further destabilized the 2 : 1 complex, possibly due to greater steric bulk. Linear alkyl chains maintained a linear and compact molecular geometry, facilitating optimal coordination and favoring the formation of 2 : 1 complexes. Conversely, branching introduced additional steric volume, interfering with effective ligand packing around the light lanthanide metal center and thus hindering higher-order complex formation. For Gd(III), all ligands exhibited slope values close to 1, indicating predominant 1 : 1 complex formation. This trend aligns with previous observations for Eu(III), suggesting that middle lanthanides generally favor a 1 : 1 coordination mode.[34] In the case of Er(III), slope values were approximately 0.5, deviating from conventional coordination behavior. This anomaly may be attributed to the co-extraction of nitrate ions and the extremely low extraction efficiency for heavy lanthanides, potentially leading to saturation effects or underestimation of slope values.[40]

UV–vis spectroscopy titration

Titration experiments of the four ligands with La(III), Eu(III), and Lu(III) were conducted in a mixed solvent system of chloroform and methanol to investigate coordination behavior across the lanthanide series in a homogeneous phase. UV–vis titration spectra and the $\log\beta$ were obtained to examine trends related to the three representative ions. For **L1**, similar spectral changes were observed upon titration with La(III), Eu(III), and Lu(III), indicating a consistent coordination rule across the three ions. As shown in Fig. 4, the absorption peaks near 294.0 nm, 326.0 nm, and 340.0 nm gradually decreased in intensity, accompanied by the emergence of new peaks around 301.0 nm and 357.0 nm. The presence of four isosbestic points in all three titration profiles confirmed the formation of new complexes. Titration experiments for **L2–L4** with the same three metal ions were also conducted, and the corresponding spectra are presented in Fig. S12. The observed spectral changes closely resembled those of **L1**, suggesting that variations in alkyl chain length or branching on the amide substituent did not significantly alter the complexation mode in homogeneous solution.

Although the stoichiometries of the metal to ligands varied across light, middle, and heavy lanthanides in the extraction slope experiments, the titration data fitting using Hypspec software revealed that only 1 : 1 complexes consistently provided the best fit for all four ligands with La(III), Eu(III), and Lu(III) in homogeneous solution. All fitting deviations were within 0.03, indicating high model reliability (Table 1). This discrepancy between homogeneous and biphasic systems may be attributed to the absence of interfacial effects and phase-transfer dynamics in solution, which likely attenuate differences in ligand–metal interaction strength observed during extraction.[42] Moreover, the affinity of these ligands for metal ions followed the order La(III) > Eu(III) > Lu(III), consistent with the trend in extraction efficiency. For the three metal ions, the ligands exhibited this stability sequence: **L1** > **L3** > **L2** > **L4**. This correlation suggests that the coordination strength decreased with the increasing length of the alkyl chain on the amide group. Furthermore, compared to the straight-chain ligand **L3** with the same number of carbon atoms, the branched substituent in **L2** further reduced the binding affinity, possibly attributed to increased steric hindrance, which hindered the optimal orientation and coordination of the ligand around the metal center. All fitted $\log\beta$ values exceeded 5, surpassing those reported for other phenanthroline-based N,O-donor ligands such as Et-Tol-DAPhen and PDAM by at least one logarithmic unit,[43,44] indicating substantially greater complex stability with f-block metal ions.

ESI-MS

ESI-MS analysis of the complex solutions provided detailed information on the species. The ESI-MS spectra of the com-

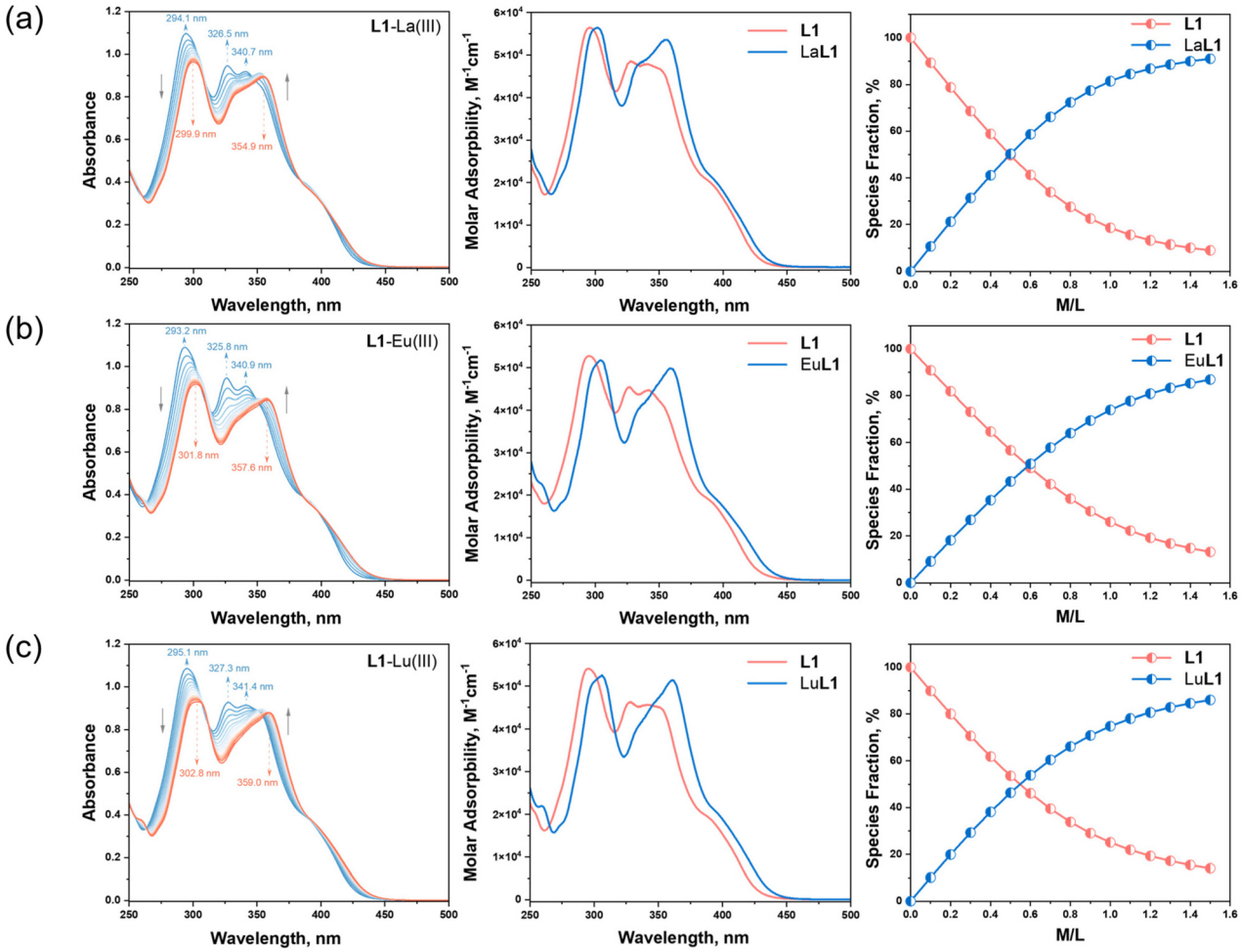

Fig. 4 UV–vis titration of **L1** with (a) La(III), (b) Eu(III), and (c) Lu(III). Left column: the changes in UV–vis titration spectra; middle column: the molar absorptivity of the species; right column: the species distribution diagrams.

Table 1 log β of the complexes

Ligands	Reaction	log β	Deviation
L1	L + La(III) → La(III)L	5.84	0.02
L2		5.72	0.03
L3		5.83	0.007
L4		5.62	0.03
L1	L + Eu(III) → Eu(III)L	5.78	0.02
L2		5.68	0.03
L3		5.76	0.03
L4		5.45	0.02
L1	L + Lu(III) → Lu(III)L	5.61	0.005
L2		5.52	0.03
L3		5.60	0.03
L4		5.39	0.006

plexes formed by the four ligands with La(III), Eu(III), and Lu(III) were measured. The comparison of the experimentally obtained m/z values with those simulated using ChemDraw is presented in Table S1. Fig. S13 shows the ESI-MS spectra of the **L1** complexes with the three metal ions.

The spectra of the **L1** complexes with the three metal ions exhibited consistent results, showing the presence of free ligand associated with either H^+ or Na^+, corresponding to $[\mathbf{L1} + H]^+$ and $[\mathbf{L1} + Na]^+$. The signal intensities of these species were higher than those of the complexes, indicating that the free ligand was the dominant species in the gas phase. Moreover, two distinct complex species were identified, corresponding to $[ML(NO_3)_2]^+$ and $[ML_2(NO_3)]^{2+}$. However, the UV–vis fitting results indicate that only 1 : 1 ligand-to-metal complexes were present in the homogeneous solution. The 2 : 1 ligand-to-metal complexes observed in the ESI-MS spectra may result from the dimerization of **L1** in solution and the gas phase, allowing the metal ion to coordinate with the dimeric ligand form.[34,45,46]

X-ray single-crystal diffraction analysis

The single-crystal structure of the complex provides clear and direct insights into the coordination environment. We found that nitrate complexes of **L1** with light and medium lanthanide elements readily form precipitates or microcrystals that are

challenging to analyze. Therefore, $Er(NO_3)_3{\cdot}6H_2O$ was selected as a representative heavy lanthanide, allowing the single-crystal structure of the 1 : 1 **L1**–Er complex to be successfully obtained. In addition, the perchlorate ion, with its weaker coordination ability compared to the nitrate,[47] resulted in the formation of the 2 : 1 **L1**–Eu complex. The detailed structural information of the corresponding single crystals is provided in Table S2.

The 1 : 1 complex between **L1** and Er(III) was composed of $Er(\mathbf{L1})(NO_3)_3$, in which Er(III) exhibited a 10-coordinate configuration, coordinating with two nitrogen atoms and two oxygen atoms from **L1**, as well as six oxygen atoms from three nitrate ions (Fig. 5a and b). Due to the lactam structure of the ligand, no conformational inversion was required during the coordination process, allowing the ligand to coordinate with Er(III) directly. In its free form, the oxygen atoms of the amide group were positioned on opposite sides of the phenanthroline plane in the lowest energy conformation (Fig. S14). However, upon coordination with Er(III), the directions of the two lactam oxygen atoms shifted to the same side of the phenanthroline plane, with the average deviation angle increasing from 0.08° to 3.65°. This suggests that while the ligand structure was fully preorganized, it can still undergo slight adjustments to facilitate coordination with the metal ions. In the complex, the average bond lengths of Er–N_{Phen}, Er–O_{amide}, and Er–$O_{nitrate}$ were 2.56 Å, 2.42 Å, and 2.44 Å, respectively. These results demonstrated that the Er–O bond lengths, both from the nitrate and the ligand, were shorter than the Er–N bond length, indicating a stronger affinity of oxygen for Er(III) than nitrogen.

The 2 : 1 complex formed between **L1** and Eu(III) has the composition $[Eu(\mathbf{L1})_2](ClO_4)_3$ (Fig. 5c and d), in which Eu(III) adopted a 8-coordinate configuration, with three perchlorate ions in the outer coordination sphere to balance the charge. Each **L1** coordinated to Eu(III) through two nitrogen atoms from the phenanthroline and two oxygen atoms from the lactam groups. Additionally, the deviation direction of the lactam oxygen atoms and the bond length pattern in $[Eu(\mathbf{L1})_2](ClO_4)_3$ were similar to those in $Er(\mathbf{L1})(NO_3)_3$. However, the coordination bond lengths between Eu(III) and the ligand atoms were longer than those of Er(III) (Eu–N_{Phen} and Eu–O_{amide}, were 2.68 Å and 2.50 Å, respectively).[48]

Although the coordination bond lengths between **L1** and Er(III)/Eu(III) were longer than or nearly equivalent to those in the corresponding DAPhen complexes,[49–51] BLPhen exhibited a markedly stronger affinity for lanthanides. This indicates that coordination bond length was not the determining factor for lanthanide binding in these ligand systems. Instead, the

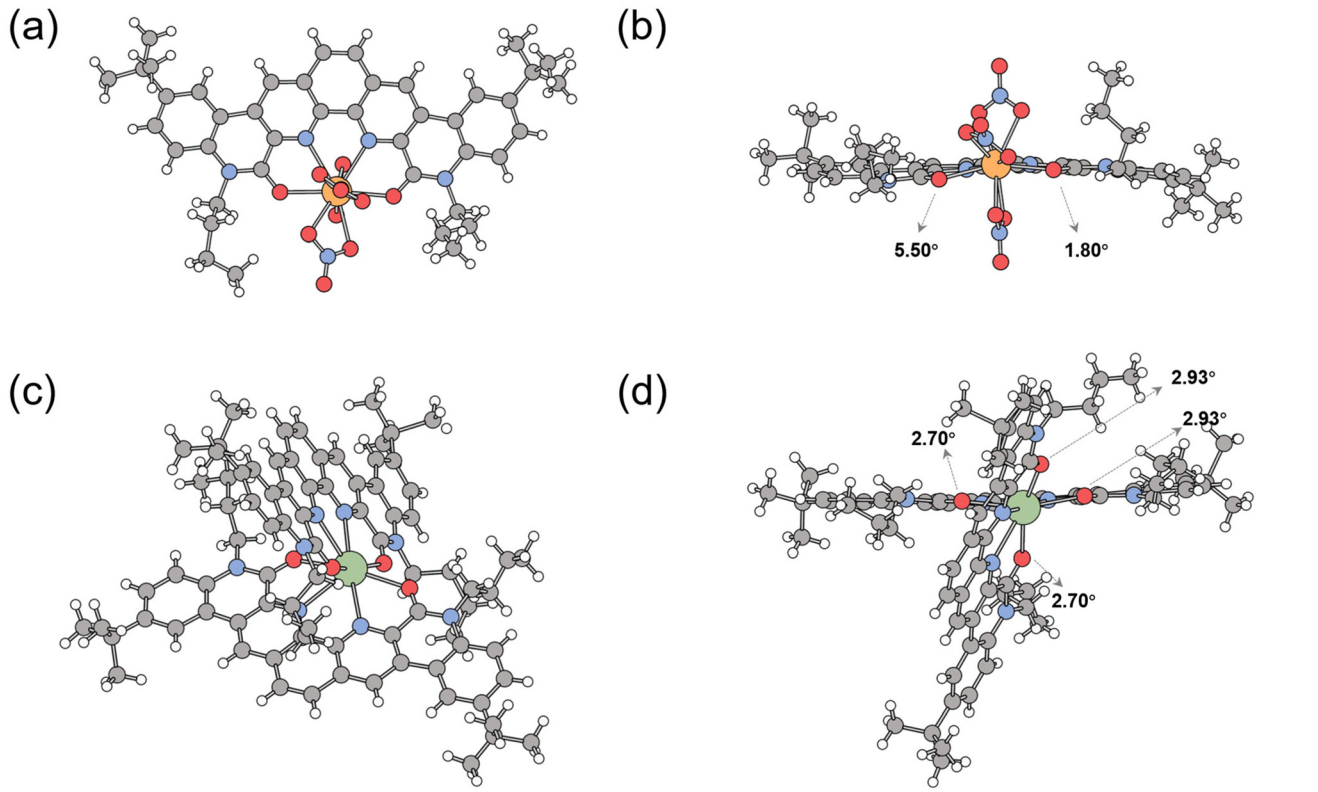

Fig. 5 (a) Crystal structure of $Er(\mathbf{L1})(NO_3)_3$, (b) torsional angles of the lactam oxygen atom deviating from the phenanthroline plane for $Er(\mathbf{L1})(NO_3)_3$, (c) coordination environment of Eu(III) in $[Eu(\mathbf{L1})_2](ClO_4)_3$ and (d) torsional angles of the lactam. Oxygen atom deviating from the phenanthroline plane for $Eu(\mathbf{L1})_2(ClO_4)_2$.

enhanced affinity of BLPhen was primarily attributed to its pre-organized molecular structure, which minimized the energetic cost associated with conformational reorganization during metal coordination.

Conclusions

In this study, four BLPhen ligands with varying alkyl substituents were designed and synthesized to investigate the influence of alkyl chain length and branching on the extraction and coordination behavior toward trivalent lanthanides. Extraction experiments at different HNO_3 concentrations indicate that the extraction trend of BLPhen for lanthanides was predominantly controlled by the size of the coordination cavity. Variations in alkyl chain length and branching did not alter the extraction trends of the BLPhen ligands toward lanthanides but affected the extraction efficiency. The extraction capability followed the order **L1** > **L3** > **L2** > **L4**. Furthermore, ligands with longer linear chains (**L3** and **L4**) displayed a more pronounced tetrad effect in the extraction patterns. On the other hand, under 1.0 M HNO_3, the $SF_{Nd(III)/Ho(III)}$ could exceed 500, demonstrating the potential for effective group separation of lanthanide elements. Slope analysis reveals that the stoichiometries of the complexes formed between the ligands and Nd(III), Gd(III), and Er(III) were not identical, with slopes of 1–2.2, 1, and 0.5, respectively. However, UV–vis titration in homogeneous solution confirmed uniform 1 : 1 complexation for all metal–ligand systems. The stability constants ($\log\beta$) followed the order **L1** > **L3** > **L2** > **L4**, consistent with extraction data, and decreased from La(III) to Lu(III). Er(**L1**)$(NO_3)_3$ and [Eu(**L1**)$_2$]$(ClO_4)_3$ offered clear coordination information. The pre-organized ligand structure restricted rotational flexibility, thereby reducing the energetic cost of conformational rearrangement during coordination and resulting in enhanced complex stability. Overall, this study highlights the crucial role of alkyl substituent geometry in regulating the coordination strength and selectivity of BLPhen ligands, providing a structural basis for the rational design of high-performance extractants for rare earth separation.

Experimental

General

All chemicals used in this study, including lanthanide nitrate hydrates, tetraethylammonium nitrate (Et_4NNO_3), and other reagents for organic synthesis, were purchased from commercial suppliers and used without further purification. The diluent used in the solvent extraction experiments, 1,2-dichloroethane (1,2-DCE), was of analytical reagent (AR) grade. For UV–vis spectroscopy titration experiments, chloroform (AR grade) and methanol (HPLC grade) were employed. Due to the radioactive toxicity of Pm, this study excluded this lanthanide metal ion.

Organic synthesis

All ligands were synthesized according to the procedure described in our previous work.[34] The synthetic route is shown in Fig. 6. Detailed synthesis and structural characterization are provided in the SI.

Solvent extraction

For the experiments at varying HNO_3 concentrations (0.001–4.0 M), the organic phase was prepared by dissolving each ligand (1.0 mM) in 1,2-DCE, while the aqueous phase was prepared by dissolving a mixture of trivalent lanthanides (total concentration: 1.4 mM, each at 0.1 mM) in HNO_3 solutions. Equal volumes of the organic and aqueous phases were transferred into 10.0 mL centrifuge tubes and mixed using a vortex shaker at 2000 rpm for 30 minutes to ensure thorough phase contact and equilibration. Following mixing, the two phases were separated by centrifugation at 3000 rpm for 3 minutes. The concentrations of metal ions in the aqueous phase, both before and after extraction, were determined using inductively coupled plasma optical emission spectrometry (ICP-OES, iCAP™ PRO, Thermo Fisher Scientific Inc., USA).

Extraction experiments at varying ligand concentrations were conducted at a fixed HNO_3 concentration of 1.0 M. Representative lanthanides from the light, middle, and heavy regions—Nd(III), Gd(III), and Er(III), respectively—were selected for slope analysis. For Nd(III) and Gd(III), the experiments were performed using ligand concentrations of 0.2, 0.4, 0.6, 0.8, and 1.0 mM. Due to the relatively low extraction efficiency of the ligands for heavy lanthanides, substantial deviations in distribution ratios could arise at lower ligand concentrations, potentially resulting in inaccurate slope determination. Therefore, the slope experiments for Er(III) were conducted at higher ligand concentrations of 1.0, 1.2, 1.4, 1.6, and 2.0 mM. All other extraction conditions were consistent with those described in the HNO_3 concentration experiments.

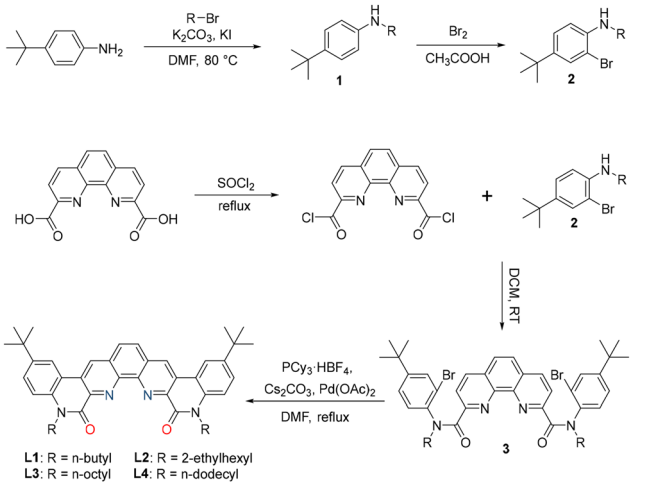

Fig. 6 Synthetic route of the ligands.

UV–vis spectroscopy titration

UV–vis titration experiments were carried out using a Shimadzu UV-2700 spectrophotometer. La(III), Eu(III), and Lu(III) were selected as representative lanthanides to investigate their complexation behavior with the four synthesized ligands. Ligand solutions (0.02 mM) and metal ion solutions (0.2 mM) were prepared in a chloroform/methanol mixture (v/v = 2 : 1) to ensure adequate solubility of the resulting metal–ligand complexes. For each titration, 2.0 mL of the ligand solution was placed in a 1.0 cm path length quartz cuvette, and 10.0 μL aliquots of the metal ion solution were added incrementally until the UV–vis absorption spectra no longer changed. The absorption spectra were recorded on 250–500 nm, as the characteristic absorption peaks of the ligands lay within this range. Spectral data were analyzed using HypSpec software[52] to calculate the $\log\beta$ of the corresponding metal–ligand complexes.

Electrospray ionization mass spectrometry (ESI-MS)

ESI-MS analyses were performed on an Agilent 6545 mass spectrometer. Solutions of the ligand and hydrated nitrates of La(III), Eu(III) and Lu(III) were prepared in a mixed solvent system consisting of HPLC-grade acetonitrile and chloroform, with both components adjusted to a concentration of 1.0 mM. The solutions were mixed and sonicated for 2–3 minutes to facilitate complex formation,[34] and then diluted fivefold to obtain the samples for analysis.

X-ray single-crystal diffraction

X-ray single-crystal diffraction was carried out on a Bruker D8 Venture system and the refinement was performed using APEX3 (Bruker) and Olex2-1.2. Additionally, disorder modeling was performed by splitting the carbon atoms of the *t*-butyl and *n*-butyl groups into two components. Single crystals of **L1** with $Er(NO_3)_3{\cdot}6H_2O$ in a 1 : 1 ratio were grown by the solvent evaporation method. Solutions of **L1** and $Er(NO_3)_3{\cdot}6H_2O$ were prepared in a chloroform–methanol mixture, and the two components were mixed and placed in a 3.0 mL vial. The mixture was allowed to stand at room temperature for several days, yielding pale yellow crystals. For the 2 : 1 type single crystals of **L1** with $Eu(ClO_4)_3$, the solvent diffusion method was employed. Solutions of **L1** and $Eu(ClO_4)_3$ were prepared in a chloroform–methanol mixture and then combined in equal volumes in a 3.0 mL vial. This vial was placed inside a 20.0 mL vial containing 1.5 mL of diethyl ether and sealed. The system was left undisturbed at room temperature for 3 days, resulting in high-quality yellow crystals suitable for X-ray diffraction analysis. Due to the small size of the **L1**–Er complex crystal, the data resolution was limited, resulting in a relatively high R_{int} value and a data completeness cutoff slightly below the recommended threshold; however, the cutoff at $2\theta = 110°$ was still marginally acceptable. Nevertheless, the crystallographic data did not affect the reliability of the structural determination. $Eu(ClO_4)_3$ was prepared by mixing an excess of Eu_2O_3 with 1.0 M $HClO_4$ and stirring the mixture at 90 °C for 3 hours.[53] The unreacted solid was then filtered off, and the filtrate was evaporated to dryness and subsequently vacuum-dried to obtain colorless crystals.

Conflicts of interest

There are no conflicts to declare.

Data availability

All the data needed to evaluate the conclusions in this work are present in the article or the supplementary information (SI). Supplementary information: ESI-HRMS, ^{1}H NMR results, synthesis procedures and characterization methods. See DOI: https://doi.org/10.1039/d5dt03012a.

CCDC 2512427 and 2456431 contain the supplementary crystallographic data for this paper.[54a,b]

Acknowledgements

This work was financially supported by the National Natural Science Foundation of China (22476178 and 22506177), the Zhejiang Provincial Natural Science Foundation of China (LRG25B060002), and the Research Funds of the Institute of Zhejiang University-Quzhou (IZQ2025RCZX003). We gratefully acknowledge Dr Xiaoyan Xiao (School of Materials Science and Engineering, Zhejiang University) and Xu Zhang (School of Chemistry and Chemical Engineering, Huaiyin Normal University) for their assistance with the single-crystal experiments.

References

1 T. Zhao, W. Li, S. Kelebek, Y. Choi, C. Wu, W. Zhang, C. Wang, Z. Zhao and F. Sadri, A comprehensive review on rare earth elements: Resources, technologies, applications, and prospects, *Rare Met.*, 2025, **44**, 7011–7040.
2 F. F. Khoury, B. S. Heater, D. R. Marzolf, S. Abeyrathna, J. W. Picking, P. Kumar, S. A. Higgins, R. Jones, A. T. Lewis, K. H. Kucharzyk and S. Banta, Mining peptides for mining solutions: Evaluation of calcium-binding peptides for rare earth element separations, *Chem. Sci.*, 2025, **16**, 15333–15346.
3 C. O. Iloeje, F. Tesfaye, A. E. Anderson and J. Hamuyuni, Recovery of rare earth and critical metals from unconventional sources, *JOM*, 2022, **74**, 990–992.
4 X. Sun, J. R. Bell, H. Luo and S. Dai, Extraction separation of rare-earth ions via competitive ligand complexations between aqueous and ionic-liquid phases, *Dalton Trans.*, 2011, **40**, 8019.
5 V. Balaram, Rare earth elements: A review of applications, occurrence, exploration, analysis, recycling, and environmental impact, *Geosci. Front.*, 2019, **10**, 1285–1303.

6 D. M. Driscoll, F. D. White, S. Pramanik, J. D. Einkauf, B. Ravel, D. Bykov, S. Roy, R. T. Mayes, L. H. Delmau, S. K. Cary, T. Dyke, A. Miller, M. Silveira, S. M. Vancleve, S. M. Davern, S. Jansone-Popova, I. Popovs and A. S. Ivanov, Observation of a promethium complex in solution, *Nature*, 2024, **629**, 819–823.
7 A. Jordens, Y. P. Cheng and K. E. Waters, A review of the beneficiation of rare earth element bearing minerals, *Miner. Eng.*, 2013, **41**, 97–114.
8 M. K. Jha, A. Kumari, R. Panda, J. R. Kumar, K. Yoo and J. Y. Lee, Review on hydrometallurgical recovery of rare earth metals, *Hydrometallurgy*, 2016, **165**, 2–26.
9 S. V. S. H. Pathapati, M. L. Free and P. K. Sarswat, A comparative study on recent developments for individual rare earth elements separation, *Processes*, 2023, **11**, 2070.
10 R. K. Jyothi, T. Thenepalli, J. W. Ahn, P. K. Parhi, K. W. Chung and J. Lee, Review of rare earth elements recovery from secondary resources for clean energy technologies: Grand opportunities to create wealth from waste, *J. Cleaner Prod.*, 2020, **267**, 122048.
11 A. B. Patil, R. P. W. J. Struis and C. Ludwig, Opportunities in critical rare earth metal recycling value chains for economic growth with sustainable technological innovations, *Circ. Econ. Sustainability*, 2023, **3**, 1127–1140.
12 T. Dutta, K. Kim, M. Uchimiya, E. E. Kwon, B. Jeon, A. Deep and S. Yun, Global demand for rare earth resources and strategies for green mining, *Environ. Res.*, 2016, **150**, 182–190.
13 I. Fidelis and J. Krejzler, Separation factors of lanthanides extracted with dibutylphosphate, *J. Radioanal. Chem.*, 1976, **31**, 45–60.
14 L. Xu, X. Yang, A. Zhang, C. Xu and C. Xiao, Separation and complexation of f-block elements using hard-soft donors combined phenanthroline extractants, *Coord. Chem. Rev.*, 2023, **496**, 215404.
15 X. Yang, L. Xu, D. Fang, A. Zhang and C. Xiao, Progress in phenanthroline-derived extractants for trivalent actinides and lanthanides separation: Where to next?, *Chem. Commun.*, 2024, **60**, 11415–11433.
16 N. V. Thakur, Separation of rare earths by solvent extraction, *Miner. Process. Extr. Metall. Rev.*, 2000, **21**, 277–306.
17 S. V. S. H. Pathapati, M. L. Free and P. K. Sarswat, A comparative study on recent developments for individual rare earth elements separation, *Processes*, 2023, **11**, 2070.
18 S. Pramanik, S. Kaur, I. Popovs, A. S. Ivanov and S. Jansone-Popova, Emerging rare earth element separation technologies, *Eur. J. Inorg. Chem.*, 2024, **27**, e202400064.
19 P. Di Bernardo, A. Melchior, M. Tolazzi and P. L. Zanonato, Thermodynamics of lanthanide(III) complexation in non-aqueous solvents, *Coord. Chem. Rev.*, 2012, **256**, 328–351.
20 K. L. Nash and M. P. Jensen, Analytical-scale separations of the lanthanides: A review of techniques and fundamentals, *Sep. Sci. Technol.*, 2001, **36**, 1257–1282.
21 R. J. Ellis, D. M. Brigham, L. Delmau, A. S. Ivanov, N. J. Williams, M. N. Vo, B. Reinhart, B. A. Moyer and V. S. Bryantsev, "Straining" to separate the rare earths: How the lanthanide contraction impacts chelation by diglycolamide ligands, *Inorg. Chem.*, 2017, **56**, 1152–1160.
22 X. Yang, L. Xu, A. Zhang and C. Xiao, Organophosphorus extractants: A critical choice for actinides/lanthanides separation in nuclear fuel cycle, *Chem. – Eur. J.*, 2023, **29**, e202300456.
23 S. Wang, X. Yang, L. Xu and C. Xiao, Separation and complexation of lanthanides with an acidic phenanthroline carboxamide ligand: Extraction, spectroscopy, and crystallography, *Ind. Eng. Chem. Res.*, 2024, **63**, 10773–10781.
24 L. Xu, X. Yang, Z. Wang, S. Wang, M. Sun, C. Xu, X. Zhang, L. Lei and C. Xiao, Unfolding the extraction and complexation behaviors of trivalent f–block elements by a tetradentate N,O-hybrid phenanthroline derived phosphine oxide ligand, *Inorg. Chem.*, 2021, **60**, 2805–2815.
25 X. Yang, P. Ren, Q. Yang, J. Geng, J. Zhang, L. Yuan, H. Tang, Z. Chai and W. Shi, Strong periodic tendency of trivalent lanthanides coordinated with a phenanthroline-based ligand: Cascade countercurrent extraction, spectroscopy, and crystallography, *Inorg. Chem.*, 2021, **60**, 9745–9756.
26 M. Simonnet, T. Kobayashi, K. Shimojo, K. Yokoyama and T. Yaita, Study on phenanthroline carboxamide for lanthanide separation: Influence of amide substituents, *Inorg. Chem.*, 2021, **60**, 13409–13418.
27 M. Simonnet, Y. Sasaki and T. Yaita, Combining a lipophilic phenanthroline carboxamide and a hydrophilic diglycolamide to increase the separation factors of adjacent light lanthanides, *Solvent Extr. Ion Exch.*, 2023, **41**, 857–867.
28 D. Fang, X. Yang, F. Gao and C. Xiao, Straightforward and versatile construction of phenanthroline-derived diamide ligands for f-block element extraction, *Chin. Chem. Lett.*, 2026, **37**, 111252.
29 N. Tsutsui, Y. Ban, H. Suzuki, M. Nakase, S. Ito, Y. Inaba, T. Matsumura and K. Takeshita, Effects of diluents on the separation of minor actinides from lanthanides with tetradodecyl-1,10-phenanthroline-2,9-diamide from nitric acid medium, *Anal. Sci.*, 2020, **36**, 241–245.
30 M. Alyapyshev, J. Ashina, D. Dar'in, E. Kenf, D. Kirsanov, L. Tkachenko, A. Legin, G. Starova and V. Babain, 1,10-Phenanthroline-2,9-dicarboxamides as ligands for separation and sensing of hazardous metals, *RSC Adv.*, 2016, **6**, 68642–68652.
31 M. R. Healy, A. S. Ivanov, Y. Karslyan, V. S. Bryantsev, B. A. Moyer and S. Jansone-Popova, Efficient separation of light lanthanides(III) by using bis–lactam phenanthroline ligands, *Chem. – Eur. J.*, 2019, **25**, 6326–6331.
32 K. R. Johnson, D. M. Driscoll, J. T. Damron, A. S. Ivanov and S. Jansone-Popova, Size selective ligand tug of war strategy to separate rare earth elements, *JACS Au*, 2023, **3**, 584–591.
33 Y. Karslyan, F. V. Sloop, L. H. Delmau, B. A. Moyer, I. Popovs, A. Paulenova and S. Jansone-Popova, Sequestration of trivalent americium and lanthanide nitrates with bis-lactam-1,10-phenanthroline ligand in a hydrocarbon solvent, *RSC Adv.*, 2019, **9**, 26537–26541.

34 F. Gao, X. Xu, X. Yang, H. Cao, D. Fang, L. Xu, C. Xu and C. Xiao, Completely preorganized bis-lactam-1,10-phenanthroline ligands with high stability for efficient separation of Am(III) over Eu(III), *Dalton Trans.*, 2025, **54**, 2871–2876.

35 S. Pramanik, B. Li, D. M. Driscoll, K. R. Johnson, B. R. Evans, J. T. Damron, A. S. Ivanov, D. E. Jiang, J. Einkauf, I. Popovs and S. Jansone-Popova, Tetradentate ligand's chameleon-like behavior offers recognition of specific lanthanides, *J. Am. Chem. Soc.*, 2024, **146**, 25669–25679.

36 M. Alyapyshev, J. Ashinab, D. Dar'In, E. Kenf, D. Kirsanov, L. Tkachenko, A. Legin, G. Starova and V. Babain, 1,10-Phenanthroline-2,9-dicarboxamides as ligands for separation and sensing of hazardous metals, *RSC Adv.*, 2016, **6**, 68642–68652.

37 N. Tsutsui, Y. Ban, H. Suzuki, M. Nakase, S. Ito, Y. Inaba, T. Matsumura and K. Takeshita, Effects of diluents on the separation of minor actinides from lanthanides with tetradodecyl-1,10-phenanthroline-2,9-diamide from nitric acid medium, *Anal. Sci.*, 2020, **36**, 241–245.

38 M. Nakase, T. Kobayashi, H. Shiwaku, S. Suzuki, T. S. Grimes, B. J. Mincher and T. Yaita, Relationship between structure and coordination strength of N and N,O-hybrid donor ligands with trivalent lanthanides, *Solvent Extr. Ion Exch.*, 2018, **36**, 633–646.

39 J. G. Bünzli, Review: Lanthanide coordination chemistry: From old concepts to coordination polymers, *J. Coord. Chem.*, 2014, **67**, 3706–3733.

40 S. Wang, X. Yang, Y. Liu, L. Xu, C. Xu and C. Xiao, Enhancing the selectivity of trivalent actinide over lanthanide using asymmetrical phenanthroline diamide ligands, *Inorg. Chem.*, 2024, **63**, 3063–3074.

41 X. Zhang, L. Yuan, Z. Chai and W. Shi, Towards understanding the correlation between UO_2^{2+} extraction and substitute groups in 2,9-diamide-1,10-phenanthroline, *Sci. China: Chem.*, 2018, **61**, 1285–1292.

42 L. Xu, N. Pu, G. Ye, C. Xu, J. Chen, X. Zhang, L. Lei and C. Xiao, Unraveling the complexation mechanism of actinide(III) and lanthanide(III) with a new tetradentate phenanthroline-derived phosphonate ligand, *Inorg. Chem. Front.*, 2020, **7**, 1174–1726.

43 C. L. Xiao, C. Z. Wang, L. Y. Yuan, B. Li, H. He, S. Wang, Y. L. Zhao, Z. F. Chai and W. Q. Shi, Excellent selectivity for actinides with a tetradentate 2,9-diamide-1,10-phenanthroline ligand in highly acidic solution: A hard-soft donor combined strategy, *Inorg. Chem.*, 2014, **53**, 1712–1720.

44 D. Merrill, J. M. Harrington, H. Lee and R. D. Hancock, Unusual metal ion selectivities of the highly preorganized tetradentrate ligand 1,10-phenanthroline-2,9-dicarboxamide: A thermodynamic and fluorescence study, *Inorg. Chem.*, 2011, **50**, 8348–8355.

45 A. I. Voloshin, N. M. Shavaleev and V. P. Kazakov, Water enhances the luminescence intensity of β-diketonates of trivalent samarium and terbium in toluene solutions, *J. Photochem. Photobiol., A*, 2000, **134**, 111–117.

46 N. B. Cech and C. G. Enke, Practical implications of some recent studies in electrospray ionization fundamentals, *Mass Spectrom. Rev.*, 2001, **20**, 362–387.

47 X. Yang, D. Fang, L. Chen, Y. Liu, S. Wang, L. Xu, A. Zhang, J. Su, C. Xu and C. Xiao, Computation-aided development of next-generation extractants for trivalent actinide and lanthanide separation, *JACS Au*, 2024, **4**, 4744–4756.

48 S. Jansone-Popova, A. S. Ivanov, V. S. Bryantsev, F. V. Sloop, R. Custelcean, I. Popovs, M. M. Dekarske and B. A. Moyer, Bis-lactam-1,10-phenanthroline (BLPhen), a new type of preorganized mixed N,O-donor ligand that separates Am(III) over Eu(III) with exceptionally high efficiency, *Inorg. Chem.*, 2017, **56**, 5911–5917.

49 M. V. Evsiunina, P. I. Matveev, P. Kalle, E. K. Khult, P. S. Lemport, N. A. Avagyan, V. G. Petrov, Y. A. Ustynyuk and V. G. Nenajdenko, Solvent extraction and coordination properties of 1,10-phenanthroline-2,9-dicarboxylic acid diamides with alkyl-aryl substituents toward lanthanides(III) and americium(III), *Inorg. Chem.*, 2025, **64**, 3311–3325.

50 R. Meng, L. Xu, X. Yang, M. Sun, C. Xu, N. E. Borisova, X. Zhang, L. Lei and C. Xiao, Influence of a N-heterocyclic core on the binding capability of N,O-hybrid diamide ligands toward trivalent lanthanides and actinides, *Inorg. Chem.*, 2021, **60**, 8754–8764.

51 B. Chen, J. Liu, L. Lv, L. Yang, S. Luo, Y. Yang and S. Peng, Complexation of lanthanides with N,N,N′,N′-tetramethylamide derivatives of bipyridinedicarboxylic acid and phenanthrolinedicarboxylic acid: thermodynamics and coordination modes, *Inorg. Chem.*, 2019, **58**, 7416–7425.

52 P. Gans, A. Sabatini and A. Vacca, Investigation of equilibria in solution. Determination of equilibrium constants with the HYPERQUAD suite of programs, *Talanta*, 1996, **43**, 1739–1753.

53 X. Yang, L. Xu, Y. Hao, R. Meng, X. Zhang, L. Lei and C. Xiao, Effect of counteranions on the extraction and complexation of trivalent lanthanides with tetradentate phenanthroline-derived phosphonate ligands, *Inorg. Chem.*, 2020, **59**, 17453–17463.

54 (*a*) CCDC 2512427: Experimental Crystal Structure Determination, 2026, DOI: 10.5517/ccdc.csd.cc2qbd1j; (*b*) CCDC 2456431: Experimental Crystal Structure Determination, 2026, DOI: 10.5517/ccdc.csd.cc2ng3qz.